
Emergent representations in networks trained with the Forward-Forward algorithm

Niccolò Tosato^{1,*}Lorenzo Basile^{2,*}Emanuele Ballarin²Giuseppe de Alteriis^{3,4}Alberto Cazzaniga¹Alessio Ansuini¹¹AREA Science Park, Italy²University of Trieste, Italy³King's College London, UK⁴University College London, UK^{*}Equal contributions**Correspondence:**

alessio.ansuini@areasciencepark.it

Abstract

The Backpropagation algorithm, widely used to train neural networks, has often been criticised for its lack of biological realism. In an attempt to find a more biologically plausible alternative, and avoid to back-propagate gradients in favour of using local learning rules, the recently introduced Forward-Forward algorithm replaces the traditional forward and backward passes of Backpropagation with two forward passes. In this work, we show that internal representations obtained with the Forward-Forward algorithm organize into robust, category-specific *ensembles*, composed by an extremely low number of active units (high sparsity). This is remarkably similar to what is observed in cortical representations during sensory processing. While not found in models trained with standard Backpropagation, sparsity emerges also in networks optimized by Backpropagation, on the same training objective of Forward-Forward. These results suggest that the learning procedure proposed by Forward-Forward may be superior to Backpropagation in modelling learning in the cortex, even when a backward pass is used.

1 Introduction

Deep Learning is a highly effective approach to artificial intelligence, with tremendous implications for science, technology, culture, and society [1]. At its core, there is the Backpropagation (Backprop) algorithm [2], which efficiently computes the gradients necessary to optimize parameters of an artificial neural network (ANN). However, Backprop lacks biological plausibility [3], leading to many attempts to address this issue. The most recent of such, the Forward-Forward algorithm developed by G. Hinton [4], eliminates the need to propagate error derivatives and store neural activities. In a standard classification context, the application of Forward-Forward requires the designation of positive and negative data. For instance, to classify images, one could assign positive (negative) data to those images having the correct (incorrect) classification embedded via one-hot encoding at the border. The Forward-Forward algorithm then attempts to discriminate between positive and negative data by optimizing a goodness function (such as, e.g., the ℓ_2 norm of the activations), akin to contrastive learning [5]. Results have been observed [4] to be satisfactory for classification tasks on MNIST [6], a well-known supervised learning benchmark.

This work goes beyond performance, investigating strong similarities between biological and artificial

neural ensembles. Our experiments demonstrate sparseness in representations learned using Forward-Forward, and similarities to cortical ensembles found in early stages of sensory processing [7]. Neurons that form ensembles are highly specialized, and are found to activate selectively when presented with positive data, while only exhibiting minimal activation to negative data or unexpected stimuli.

When Forward-Forward is tested on a new category (unseen during training) its representations define an ensemble with similar characteristics to the ones that emerge on seen categories, the only apparent difference being a lower value of the activations. Our results also indicate that there may exist collective suppression mechanisms similar to those of biological inhibitory neurons [8]. Although optimizing the standard cross-entropy loss within the same classification task does not appear to produce the behavior we observe, it may not solely be due to the Forward-Forward algorithm. In fact, similar results are obtained by replacing Forward-Forward with Backprop, while optimizing the same goodness function. This suggests that the focus should be put on the purpose and biological meaning of the loss function rather than the training algorithm [9].

2 Related work

2.1 Forward-Forward

The Forward-Forward algorithm [4] is a newly proposed learning algorithm for artificial neural networks, whose main premise is being able to overcome the notorious biological implausibility of Backprop [2]. In fact, while its effectiveness made Backprop the standard algorithm for training neural networks, it is based on biologically unrealistic assumptions, which include the need to propagate information forwards and backwards through the network [9]. Forward-Forward owes its name to the fact that it replaces the backward pass with an additional forward pass.

The two forward passes are executed on different data, named positive and negative data. During training, the objective of Forward-Forward is to maximize a so-called goodness function of the neural activations (e.g. the ℓ_p norm) on positive data and minimize it on negative data. In a simple image classification setting, such as the one we adopt in this paper, one could encode a class label at the border of images by one-hot encoding it with a white pixel (as shown in Figure 1, panel A). Then, following the definition from [4], positive data are those for which the encoded label matches the ground truth label, while the opposite is true for negative data.

Layers are trained separately and sequentially, and learn to discriminate between positive and negative data by maximizing and minimizing their assigned goodness, according to the data presented. Crucially, activations are normalized before being passed to the subsequent layer, to prevent layers from relying on the goodness computed by their predecessors. From the biological point of view, normalization is known to be a "canonical neural computation", as highlighted by [10]. At test time, when a new unlabeled sample has to be categorized, many copies of the image are created, each with a different one-hot encoded label. These are then fed into the neural network to obtain a goodness score. Finally, the image gets classified in the category that produced the maximum goodness value. In the seminal Forward-Forward paper [4], satisfactory classification results are reported on the standard handwritten digit recognition data set MNIST, with the definition of positive and negative data cited above, and using the ℓ_2 or ℓ_1 norm of activations as goodness functions. We illustrate properties of representations obtained in Forward-Forward networks, that are reminiscent of what is found in sensory cortices, where ensembles of a few number of units activate consistently in response to different stimuli. We discuss properties of neural ensembles in the following section.

2.2 Neural Ensembles

Ensembles are defined as sparse groups of neurons that co-activate together. Remarkably, ensembles – rather than single neurons – have long been suggested to be the emergent functional blocks of cortical activity ([8, 11, 12, 13]) and have a prominent role in sensory processing, memory [14] and behavior [15]. Their importance began to be confirmed experimentally thanks to advances in the techniques to record simultaneously the activity of large numbers of neurons, especially using calcium imaging [16]. In visual processing, [7] finds that spiking activity in the cortex is dominated by ensembles, whose properties cannot be accounted for by the independent firing activities of neurons in isolation. They also find that ensembles can be both generated by sensory stimuli (visual, in this case) or by the spontaneous activity of the network; however, visually evoked ones are time-locked to stimuli. Moreover, they show that single neurons can participate in more than one ensemble, thus

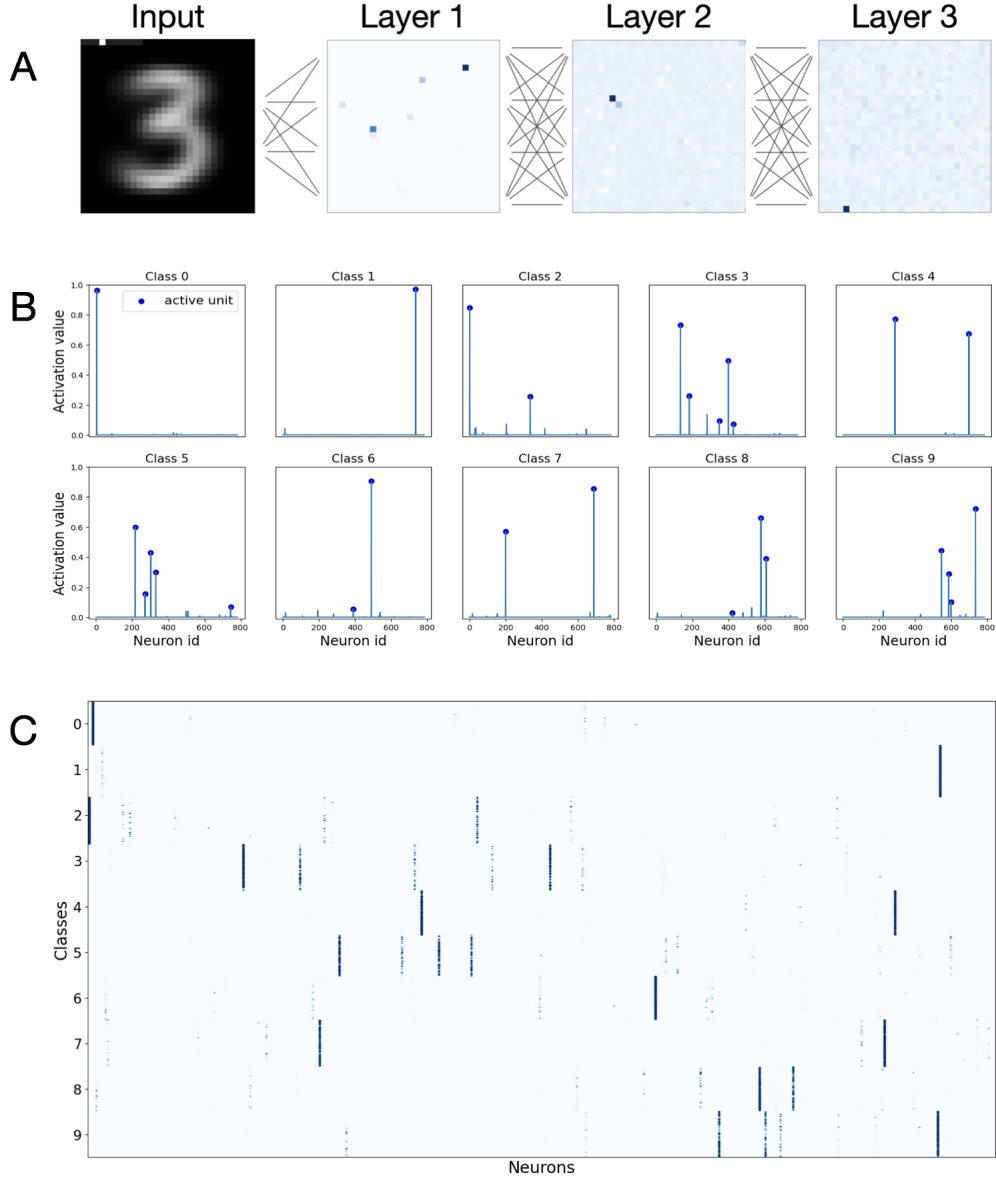


Figure 1: Activation patterns in a MLP trained on the MNIST data set, according to the Forward-Forward algorithm. Panel A: Examples of activation patterns in response to a representative input. Images show the activation value of network units reshaped to a square for clarity of representation, darker square represents more active neurons; Panel B: Each plot is the mean activation value by neuron for a class in the first layer. Horizontal axis indicates neuron index, y axis its mean activation. Blue dots indicate units that are considered active using **Method 1** with a threshold of 0.9 (see subsection 3.4); Panel C: Full activation map for the Layer 1 for all images, grouped by class. A blue dot in position (x, y) indicates that the input y activates neuron x , and colorscale represents intensity of activation.

maximizing the encoding potential of the network. Interestingly, the same ensembles are present both when reacting to stimuli and during spontaneous activity, indicating that they serve as the inherent fundamental components giving rise to visual responses.

The research presented in [17] confirms that sensory (visual) inputs activate sparse ensembles in the primary visual cortex (V1). Moreover, it shows that images can be decoded starting from a low number (ensemble) of highly responsive neurons, and that adding other neurons does not increase (or even diminishes) decoding performance. These neurons consistently and reliably encode visual

inputs across multiple trials. The study proposes that partially overlapping receptive fields play a role in achieving sparse and robust representation of information. Consequently, collecting the activity of highly responsive neurons emerges as an optimal decoding strategy for downstream neurons. Ensembles are also shown to be present in other animal models [18, 19] and a recent work shows that they may also play a role in conscious experience [20]. Regarding the duration of ensembles, [21] reveals that neuronal ensembles have the capacity to endure for weeks, suggesting that they could potentially function as a foundation for the long-term representation of perceptual states or memories. Advancements in technology have allowed not only to visualize, but also to stimulate cortical neurons [22], allowing to "play the piano" [23] with ensembles of neurons. These all-optical approaches [15] show that when a specific group of neurons in V1 of mice is repeatedly activated, it generates a coactive (imprinted) neuronal ensemble that remains spontaneously active even after a day has passed. Remarkably, the activation of certain individual neurons from these imprinted ensembles is capable of recalling the entire ensemble, showcasing the phenomenon of pattern completion. Notably, this pattern completion effect persists even a day after the initial imprinting process. Also [23] shows a causal relation between stimulation of ensembles and behavior. Finally, the idea of ensembles has inspired computational models [24]. One of them [25] shows that sparse and redundant (hence more robust) representation is optimal for encoding of natural images with unreliable neurons, as also confirmed by [26, 27].

3 Methods

In this work, we investigate the representations produced by three models:

- A Forward-Forward classifier, in the style of [4] (**FF**);
- A network whose architecture is identical to the one of **FF**, but trained end-to-end with Backpropagation to maximize the same goodness function (**BP/FF**);
- A standard classifier ANN trained with Backpropagation (**BP**).

3.1 Forward-Forward model (**FF**)

Our **FF** follows the original architectural shape proposed in [4]. It consists in 3 fully-connected layers, each composed by 784 units with sigmoid activation. During both inference and training phases, the evaluation of input data relies on layer-wise ℓ_∞ norm as the goodness function of choice. Furthermore, a ℓ_∞ normalization layer is incorporated between contiguous hidden layers. As regards the definition of positive and negative data, the one-hot technique is used to embed class labels in the images, with the top-left corner of input images hosting such label encoding. By default, these pixels are set to zero, whereas, in the case of positive data, the pixel corresponding to the ground truth class (in arbitrary, but fixed, sequential order) is assigned the maximum value observed in the image. In the case of negative examples, such value is given to one of the other pixels. Layers are trained individually, each using full batch Adam [28] optimization for 1000 epochs, with a constant learning rate of 10^{-2} .

3.2 FF-like network trained with Backpropagation (**BP/FF**)

The **FF** architecture, while designed to be optimized using the Forward-Forward algorithm, can be trained seamlessly with Backpropagation, without any major modification. Indeed, keeping the definition of positive and negative data introduced in the previous section, one could simply use Backpropagation to optimize the same goodness-based loss from the Forward-Forward algorithm. In detail, positive and negative data are fed through the network during the forward step, and the goodness function on the internal representations is evaluated. The backward pass is then executed, optimizing parameters to achieve the same objective as the Forward-Forward model. It is worth pointing out that, in this case, the goodness is maximized globally instead of layer-by-layer, i.e. locally. To maintain similarity with the setup of the **FF**, the same training configuration and parameters are utilized.

3.3 Fully connected network trained by Backpropagation on the Cross-Entropy loss (BP)

To compare the trained **FF** network results with a truly *standard* baseline, a classical neural classifier – a multilayer perceptron (MLP) – is employed. This setup shares the same number of layers, layerwise neuron count, and non-linear function choice with the **FF** and **BP/FF** models. What differentiates the **BP** model from the previous ones is the addition of a softmax classification layer after the last hidden layer to suitably shape the output for the classification task. The model is trained using the standard Cross-Entropy loss, and parameters are optimized using Adam. The training process involves 20 epochs and a learning rate of 10^{-2} is employed.

3.4 Analysis of representations

For each implemented model, we analyze the internal representation computed by each layer. For **FF** and **BP/FF** the representation are extracted after the non-linearity and before normalization. For representation analyses we only consider data belonging to the test set (i.e. unseen during training) and correctly classified (i.e. the representations relative to misclassified inputs have been discarded from our analyses).

To assess the emergence of ensembles in each model/data set combination we adopt two methods. The starting point of both methods is the computation of representation matrices (one per category) X of shape (m, n) , where m is the number of test images of the given category and n is the number of neurons in the layer.

Method 1 We compute the histogram of values in X , set a quantile in their distribution, and define a neuron as active – and therefore part of the ensemble – if its median activation (median across columns of X) exceeds the threshold. The rationale of choosing the median instead of the mean lies in its increased robustness to noisy observations.

Method 2 We compute the mean activation $\langle x \rangle$ of each neuron in X (average of columns) and then we observe that neurons with a prominent activity (the ones corresponding to the dark vertical stripes of Figure 1) should satisfy two conditions: (1) the number of other neurons having a higher activity n_h is small, and (2) their density ϱ is small. We measure the latter density introducing a radius ε and counting for each neuron activity the number of neurons with an activity level within ε , and then divide this number by $2\varepsilon^1$. In a ϱ, n_h diagram, the prominent peaks cluster in the bottom left part of the diagram and are easily isolated (see Figure 4, Panel **c**).

Regardless of the method of choice, the output of this analysis is an ensemble of active units for each category $\mathcal{E}^c = \{e_1^c, e_2^c, \dots, e_{n_c}^c\}, \forall c = 1, 2, \dots, C$, where n_c is the number of active units for category c . Once ensembles are defined, it is possible to look at units that are shared across categories c and c' by considering $\mathcal{E}^c \cap \mathcal{E}^{c'}$. In all of our experiments we adopt **Method 1** to define ensembles, with the exception of the results reported in Figure 4. In such case, **Method 2** is adopted due to its increased sensitivity in order to detect the weaker activations of categories unseen during training. In all other experiments the results given by the two methods are qualitatively similar (see Appendix for more details and a comparison between the two Methods).

3.5 Computational Resources

The training procedure and subsequent experiments were conducted on a NVIDIA DGX A100 system. The DGX A100 is equipped with 8 NVIDIA A100 GPUs that are interconnected using NVLink technology. Each GPU is equipped with 6912 CUDA cores, 432 Tensor core and 40 GB of high-bandwidth memory.

3.6 Data

The data sets we use to train and test the networks are MNIST [6] and FASHIONMNIST [29]. The MNIST data set consists of a collection of handwritten Arabic numerals, from 0 to 9, each represented as a grayscale image of size 28×28 . The FASHIONMNIST data set is designed as a drop-in replacement to the classical MNIST data set, offering a more challenging task that requires classifying images of various clothing items into different categories. Similar to MNIST, the FASHIONMNIST data set consists of grayscale images with a resolution of 28×28 pixels, belonging to a total of 10

¹ Except when $\langle x \rangle + \varepsilon > 1$: in this case we divided the count by $\varepsilon + \min(\varepsilon, 1 - \langle x \rangle)$

different classes, each representing a specific type of clothing item. Both data sets exhibit balanced categories, with 60000 training images and 10000 test images.

4 Results

We describe the results of our models on MNIST and FASHIONMNIST; this gives us the opportunity to outline some properties of the representations that emerge with the peculiar learning procedure of **FF**. These properties (such as the emergence of category-specific ensembles that represent stimuli and the fact that ensembles can share units) establish a link between neural networks trained with Forward-Forward and what is observed in biological neural networks and described in subsection 2.2.

4.1 Classification accuracy

Before delving into the main results of this work, and analysing the internal representations learned by our proposed models, we assess how well they perform on the classification tasks at hand. Table 1 contains the results in terms of classification accuracy for all models we tested (**FF**, **FF/BP** and **BP**) on both MNIST and FASHIONMNIST. While these values are far from the state-of-the-art (0.9965 [30] and 0.8770 [29] respectively, for fully-connected networks), they are sufficiently high to ensure that the networks are effectively capturing structure in data, thus reinforcing our subsequent investigations.

Table 1: Classification accuracy. Means and standard errors were computed on 15 runs for each configuration.

Model	MNIST		FASHIONMNIST	
	Mean	Std. Err.	Mean	Std. Err.
FF	0.93	$1.0 \cdot 10^{-3}$	0.78	$7.3 \cdot 10^{-3}$
BP/FF	0.79	$1.2 \cdot 10^{-3}$	0.79	$8.1 \cdot 10^{-3}$
BP	0.77	$7.6 \cdot 10^{-2}$	0.82	$2.5 \cdot 10^{-3}$

4.2 Forward-Forward elicits sparse neural ensembles

The models **FF** and **BP/FF**, which are based on the original Forward-Forward network architecture, exhibit activations of small ensembles, which are similar to the ones observed in sensory cortices for information representation [8, 7, 12]. Figure 1 shows the activations of neurons in Layer 1 of the network and highlights the emergence of sparse ensembles (see Appendix A.1 for a visualization of the activations in Layers 2 and 3). These representations involve a remarkably low number of active units: the average ensemble size in the **FF** model trained on the MNIST data set is 2.69 units for Layer 1, 5.49 for Layer 2 and 1.47 for Layer 3. Similar results are shown for the FASHIONMNIST data set (see Table 2), with a larger ensemble population, speculatively due to the higher complexity of the classification task. The emergence of ensembles is also visible in the **BP/FF** model, although the number of active units per ensemble is always higher than the corresponding one found for **FF** (see Table 2). In both instances, the representations exhibit significantly less sparsity compared to the baseline established by the standard **BP**, as reported in Table 2 and shown for each category in Figure 2

Table 2: Mean \pm standard error of the size of ensembles over 15 experiments, detected with **Method 1** and a threshold of 0.95

Model	MNIST			FASHIONMNIST		
	Layer 1	Layer 2	Layer 3	Layer 1	Layer 2	Layer 3
FF	2.7 ± 0.04	5.5 ± 0.30	1.5 ± 0.13	2.3 ± 0.07	18.2 ± 1.01	7.2 ± 0.73
BP/FF	6.1 ± 0.80	15.9 ± 2.87	38.9 ± 0.11	17.5 ± 0.53	33.9 ± 0.62	2.2 ± 0.30
BP	287.7 ± 7.82	133.4 ± 13.45	39.8 ± 0.65	304.7 ± 2.55	132.9 ± 6.65	39.0 ± 0.09

4.3 Semantically similar classes elicit ensembles with shared neurons

Drawing a parallel with a phenomenon that is observed in Neuroscience [17], semantically related categories can be expected to share units of their ensembles, and this is indeed what we observe, as

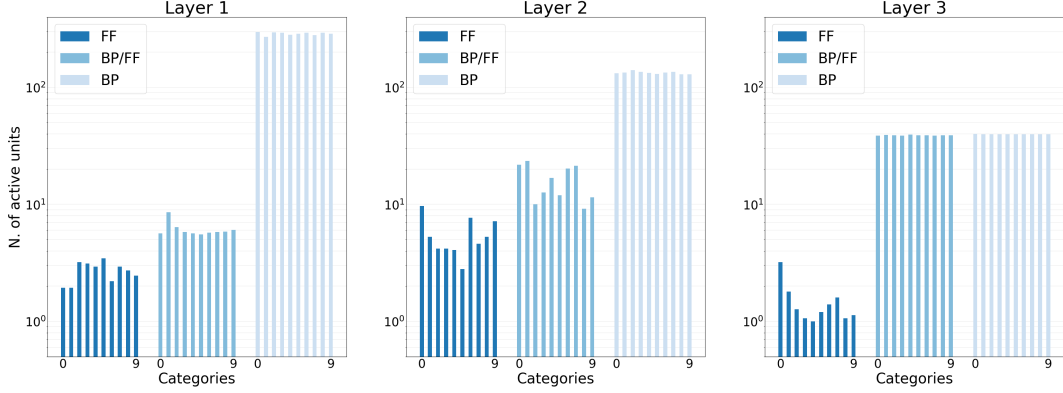


Figure 2: Average number of active units in ensembles. Ensembles are detected using **Method 1** with a threshold of 0.95, performing 15 experiments. The logarithmic y axis represents the average number of active units on MNIST data set, with category specific vertical bars. In the **BP** model such number is an order of magnitude larger than in the other models, whereas **FF** and **BP/FF** exhibit a comparable number of active units per category.

reported in Figure 3. Results are reported for FASHIONMNIST, where there exists a clear semantic relationship among classes. We observe a visible tendency towards shared units between semantically similar classes, such as T-shirt/top, pullover, coat and shirt.

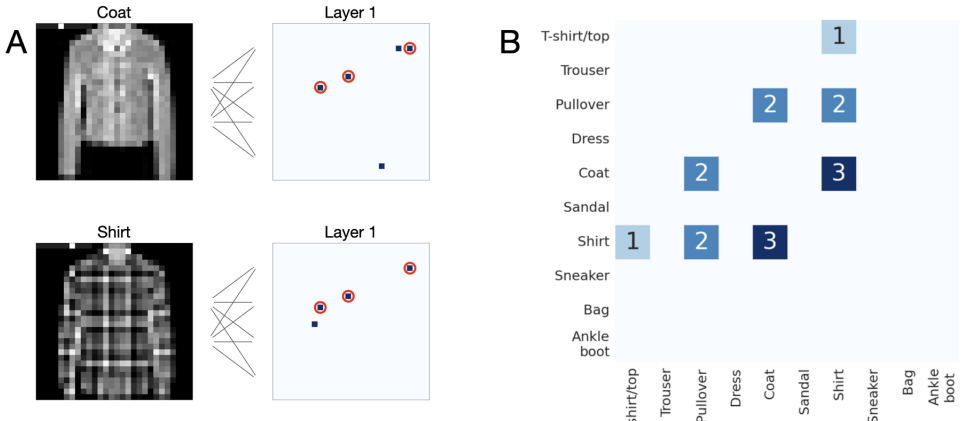


Figure 3: Semantically similar classes in FASHIONMNIST elicit ensembles with shared neurons. Panel **A**: The active units elicited by two example inputs in the first hidden layer. Units are considered active using **Method 1** with a threshold of 0.9 (see subsection 3.4). Red circles indicate the active units which are shared between the two categories. The average number of shared cells between the two categories is 1.73, calculated on 15 runs; Panel **B**: Element i,j of the matrix indicates how many units are shared between the ensembles of category i and category j on a single experiment.

4.4 Generalization to unseen categories

We check if the **FF** model, trained on a data set missing one category, is able to directly generalize on the unseen category by giving rise to a valid ensemble without the need of further training. More specifically, we train **FF** on FASHIONMNIST deprived of the first category and then extract the representation of data belonging to the unseen category.

As shown in Figure 4, we find that the network is able to generate a sparse representation, containing one active neuron, qualitatively similar to the ones elicited by the other categories seen during training, except for a lower value of the activations. The active neuron relative to the unseen category has an average activity of 0.34, while the other active neurons in the corresponding layer have an average

values of 0.43. This result relates to biological neural networks [17, 8], where ensembles appear to be the functional building block of brain representations even in the absence of known stimuli.

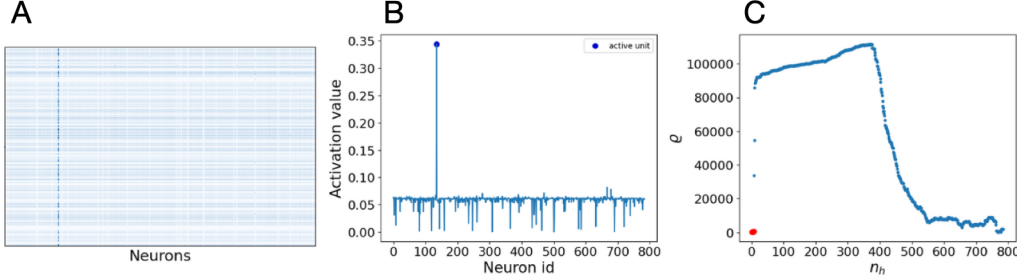


Figure 4: Panel **A**: neural activations evoked by an unseen category during the training. The prominence of a specific neuron emerges clearly; Panel **B**: average activity $\langle x \rangle$ for each neuron. The only active unit (represented with a blue dot) is detected using **Method 2** (see subsection 3.4); Panel **C**: in the decision diagram (ϱ, n_h) obtained applying **Method 2** the cluster that defines neurons of the ensemble (marked in red) is very well isolated.

4.5 Distribution of excitatory and inhibitory connections

We examine the distribution of positive and negative weights after training for the different models and data sets. We observe a sharp difference across models, with a remarkable dominance of negative weights in the case of **FF**.

The second hidden layer exhibits the most significant differences between models, as reflected by the results reported in Table 3, that indicate how neural ensembles in a layer collaborate with units in the preceding layer. Specifically, the presence of a small number of positive weights connecting the first and second hidden layers highlights the selectivity of neurons towards specific input patterns. Consequently, ensembles are separated from inactive neurons and distinct ensembles. Furthermore, positive weights reinforce connections within category ensembles. Although **BP/FF** may resemble **FF** architecture in terms of sparseness, a closer inspection of the weights suggests the potential absence of inhibitory effects and smaller subcircuit isolation. On the other hand, the results obtained from the first hidden layer do not reveal significant differences in the receptive field on the input space across different architectures.

Once again, these results make a fascinating connection to Computational Neuroscience, in which the Excitatory/Inhibitory (E/I) balance is known to play a key role in the stability of the network and in general in brain dynamics [31, 32].

Table 3: Fraction of positive weights

Model	MNIST			FASHIONMNIST		
	Layer 1	Layer 2	Layer 3	Layer 1	Layer 2	Layer 3
FF	0.63	0.002	0.035	0.44	0.012	0.038
BP/FF	0.64	0.36	0.49	0.43	0.17	0.005
BP	0.44	0.32	0.24	0.49	0.32	0.24

5 Discussion

Our main finding is that neural networks, trained with the Forward-Forward algorithm, elicit biologically plausible sparse neural ensembles [8, 7], which robustly and reliably encode information and can overlap for similar input [17]. We started by collecting and analyzing representations from **FF** networks trained on MNIST and FASHIONMNIST and defined, separately for each category, subsets of units (*ensembles*) that prominently and consistently activate in response to data in the category (subsection 4.2). These category-specific ensembles turn out to be composed of a few units, giving rise to an high representation sparsity (see Table 2), which is consistent with experimental findings in sensory cortex [7]. Furthermore, when image categories are characterized by a certain degree of visual similarity the corresponding ensembles often share one or more units (see subsection 4.3,

Figure 2). These results are consistent to what happens in sensory cortices [17], as discussed in detail in subsection 2.2, where ensembles of units (circuits) are defined.

We tested the ability of trained **FF** models to cope with new data, and we observed that the activations in response to an unseen input category formed a new ensemble, with similar characteristics of sparsity as the ones formed for other classes during training (subsection 4.4). This finding suggests that **FF** can perform well in zero-shot classification tasks, which is particularly interesting in view of the importance of zero/few-shot learning in human and animal cognitive performances [33].

While absent in the **BP** model, the existence of ensembles composed by a few units is not unique to **FF**, since it is observed also in **BP/FF** (subsection 4.2). However, despite their similarity in some characteristics of representations, the **FF** and **BP/FF** models are profoundly different, as demonstrated by a one order of magnitude difference in their fraction of negative/positive weights (Table 3).

The sparsity of representations has computational benefits for sensory processing; [27] underlines that sparsity may be the optimal encoding strategy for neuronal networks, for it is energy efficient (this is a crucial point for natural neural networks, which are limited by metabolic constraints), it increases the memory-storage capacity, and it is easier to readout at subsequent processing layers. [34] shows that sparse and expansive coding (i.e., from a lower dimensional sensory input space to a higher dimensional neural representation) reduces the intra-stimulus variability (variability of stimuli belonging to the same class), maximizes the inter-stimulus variability, and allows optimal and efficient readout of downstream neurons. This is why sparse and expansive transformations are widespread in biology, for example in rodents [35] or flies [36]. This establishes a strong link between our findings and what is observed in biological neural networks. Overall, these findings corroborate the idea that Forward-Forward might be a better model than Backprop for learning in the cortex [4]. As shown in section 4, besides being a non biological learning rule, Backprop elicits non-sparse and less biologically plausible representations.

This work is a starting point for further explorations in the field of biologically plausible representations. It is our intention to extend our experiments to larger models and data sets, exploring the possibility of scaling-up to more challenging RGB data sets such as CIFAR-10 and to widely employed image processing architectures such as Convolutional Neural Networks.

A closer inspection of the activation patterns within category will be necessary to test for the co-existence of multiple patterns, with one dominant and possibly many subdominant patterns. We did not investigate yet this *microstructure* [37], leaving it to possible extensions of this work.

Based on experimental results indicating the presence of small category-specific ensembles, typically smaller than those in other networks such as **BP**, a potential future direction for investigation could involve network pruning [38]. This process would involve reducing the layer size to create a more efficient network during the inference phase, guided by the significance of neurons in the ensembles. It may be interesting also to observe how the organization, size, and sparseness of ensembles change as training proceeds. This may provide insights into how ensembles are formed, maintained and eventually replaced, and may also be compared with neurophysiological data, to test if the biological plausibility of the ensembles extends to a dynamical setting during learning.

Another possible direction for future research would be to look for relations between the intrinsic dimension of data representation in hidden layers [39] and the size of the ensembles.

Finally, a possible future direction is to implement Forward-Forward by alternating positive and negative training phases, in what is defined as a “sleep”/“wake” alternation. A possible way to do so was sketched in [4]. The sleep-wake alternation is another possible bridge between artificial and biological networks. Indeed, neuroscientific hypotheses for sleep propose that sleep is the “price to pay for plasticity” (i.e., learning) [40]. It is thus interesting that many biologically plausible or brain inspired learning algorithms, starting from Helmholtz Machines [41] (or, for a more recent idea, see [42]) resemble the sleep-wake alternation.

Acknowledgements

We thank Alex Rodriguez (University of Trieste) for the idea of testing the models on a category unseen during training.

References

- [1] Tyna Eloundou, Sam Manning, Pamela Mishkin, and Daniel Rock. Gpts are gpts: an early look at the labor market impact potential of large language models, 2023. arXiv: 2303.10130.
- [2] David E Rumelhart, Geoffrey E Hinton, and Ronald J Williams. Learning representations by back-propagating errors. *Nature*, 323(6088):533–536, 1986.
- [3] David G. Stork. Is backpropagation biologically plausible? In *Proceedings of the International Joint Conference on Neural Networks*, 1989.
- [4] Geoffrey Hinton. The forward-forward algorithm: some preliminary investigations. *arXiv preprint arXiv:2212.13345*, 2022.
- [5] Ting Chen, Simon Kornblith, Mohammad Norouzi, and Geoffrey Hinton. A simple framework for contrastive learning of visual representations. In *Proceedings of the International Conference on Machine Learning*, 2020.
- [6] Yann LeCun and Corinna Cortes. The MNIST handwritten digit database, 2010.
- [7] Jae-eun Kang Miller, Inbal Ayzenshtat, Luis Carrillo-Reid, and Rafael Yuste. Visual stimuli recruit intrinsically generated cortical ensembles. *Proceedings of the National Academy of Sciences*, 111(38):E4053–E4061, 2014.
- [8] Rafael Yuste. From the neuron doctrine to neural networks. *Nature Reviews Neuroscience*, 16(8):487–497, 2015.
- [9] Blake A Richards, Timothy P Lillicrap, Philippe Beaudoin, Yoshua Bengio, Rafal Bogacz, Amelia Christensen, Claudia Clopath, Rui Ponte Costa, Archy de Berker, Surya Ganguli, et al. A deep learning framework for neuroscience. *Nature Neuroscience*, 22(11):1761–1770, 2019.
- [10] Matteo Carandini and David J Heeger. Normalization as a canonical neural computation. *Nature Reviews Neuroscience*, 13(1):51–62, 2011.
- [11] Donald Olding Hebb. *The organization of behavior: A neuropsychological theory*. Psychology press, 2005.
- [12] Kenneth D Harris. Neural signatures of cell assembly organization. *Nature reviews neuroscience*, 6(5):399–407, 2005.
- [13] Buzsáki György. Neural syntax: cell assemblies, synapsembles, and readers. *Neuron*, 68(3):362–385, 2010.
- [14] John J Hopfield. Neural networks and physical systems with emergent collective computational abilities. *Proceedings of the national academy of sciences*, 79(8):2554–2558, 1982.
- [15] Luis Carrillo-Reid, Shuting Han, Weijian Yang, Alejandro Akrouh, and Rafael Yuste. Controlling visually guided behavior by holographic recalling of cortical ensembles. *Cell*, 178(2):447–457, 2019.
- [16] Luis Carrillo-Reid and Vladimir Calderon. Conceptual framework for neuronal ensemble identification and manipulation related to behavior using calcium imaging. *Neurophotonics*, 9, 2022.
- [17] Takashi Yoshida and Kenichi Ohki. Natural images are reliably represented by sparse and variable populations of neurons in visual cortex. *Nature communications*, 11(1):872, 2020.
- [18] Christophe Dupre and Rafael Yuste. Non-overlapping neural networks in hydra vulgaris. *Current Biology*, 27(8):1085–1097, 2017.
- [19] Jing Liu and Scott C Baraban. Network properties revealed during multi-scale calcium imaging of seizure activity in zebrafish. *Eneuro*, 6(1), 2019.
- [20] Richard Boyce, Robin F Dard, and Rosa Cossart. Cortical neuronal assemblies coordinate with eeg microstate dynamics during resting wakefulness. *Cell Reports*, 42(2), 2023.
- [21] Jesús E. Pérez-Ortega, Tzitzitlini Alejandre-García, and Rafael Yuste. Long-term stability of cortical ensembles. *Elife*, 10:e64449, 2021.
- [22] Adam M Packer, Lloyd E Russell, Henry WP Dalgleish, and Michael Häusser. Simultaneous all-optical manipulation and recording of neural circuit activity with cellular resolution in vivo. *Nature methods*, 12(2):140–146, 2015.
- [23] Luis Carrillo-Reid and Rafael Yuste. Playing the piano with the cortex: role of neuronal ensembles and pattern completion in perception and behavior. *Current opinion in neurobiology*, 64:89–95, 2020.

- [24] Christos H Papadimitriou, Santosh S Vempala, Daniel Mitropolsky, Michael Collins, and Wolfgang Maass. Brain computation by assemblies of neurons. *Proceedings of the National Academy of Sciences*, 117(25):14464–14472, 2020.
- [25] Eizaburo Doi and Michael Lewicki. Sparse coding of natural images using an overcomplete set of limited capacity units. *Advances in Neural Information Processing Systems*, 17, 2004.
- [26] David J Field. What is the goal of sensory coding? *Neural Computation*, 6(4):559–601, 1994.
- [27] Bruno A Olshausen and David J Field. Sparse coding of sensory inputs. *Current Opinion in Neurobiology*, 14(4):481–487, 2004.
- [28] Diederik P. Kingma and Jimmy Ba. Adam: a method for stochastic optimization. In *Proceedings of the International Conference on Learning Representations*, 2017.
- [29] Han Xiao, Kashif Rasul, and Roland Vollgraf. Fashion-mnist: a novel image dataset for benchmarking machine learning algorithms, 2017. arXiv: 1708.07747.
- [30] Dan Claudiu Cireşan, Ueli Meier, Luca Maria Gambardella, and Jürgen Schmidhuber. Deep, big, simple neural nets for handwritten digit recognition. *Neural Computation*, 22(12):3207–3220, December 2010.
- [31] Wulfram Gerstner and Werner M Kistler. *Spiking neuron models: Single neurons, populations, plasticity*. Cambridge university press, 2002.
- [32] Gustavo Deco, Adrián Ponce-Alvarez, Patric Hagmann, Gian Luca Romani, Dante Mantini, and Maurizio Corbetta. How local excitation–inhibition ratio impacts the whole brain dynamics. *Journal of Neuroscience*, 34(23):7886–7898, 2014.
- [33] Brenden M Lake, Ruslan Salakhutdinov, and Joshua B Tenenbaum. Human-level concept learning through probabilistic program induction. *Science*, 350(6266):1332–1338, 2015.
- [34] Baktash Babadi and Haim Sompolinsky. Sparseness and expansion in sensory representations. *Neuron*, 83(5):1213–1226, 2014.
- [35] Peter Mombaerts, Fan Wang, Catherine Dulac, Steve K Chao, Adriana Nemes, Monica Mendelsohn, James Edmondson, and Richard Axel. Visualizing an olfactory sensory map. *Cell*, 87(4):675–686, 1996.
- [36] Glenn C Turner, Maxim Bazhenov, and Gilles Laurent. Olfactory representations by drosophila mushroom body neurons. *Journal of neurophysiology*, 99(2):734–746, 2008.
- [37] Roberto F Galán. On how network architecture determines the dominant patterns of spontaneous neural activity. *PloS one*, 3(5):e2148, 2008.
- [38] Davis Blalock, Jose Javier Gonzalez Ortiz, Jonathan Frankle, and John Guttag. What is the state of neural network pruning? *Proceedings of machine learning and systems*, 2:129–146, 2020.
- [39] Alessio Ansuini, Alessandro Laio, Jakob H Macke, and Davide Zoccolan. Intrinsic dimension of data representations in deep neural networks. *Advances in Neural Information Processing Systems*, 32, 2019.
- [40] Giulio Tononi and Chiara Cirelli. Sleep and the price of plasticity: from synaptic and cellular homeostasis to memory consolidation and integration. *Neuron*, 81(1):12–34, 2014.
- [41] Peter Dayan, Geoffrey E Hinton, Radford M Neal, and Richard S Zemel. The helmholtz machine. *Neural computation*, 7(5):889–904, 1995.
- [42] Roman Pogodin, Yash Mehta, Timothy Lillicrap, and Peter E Latham. Towards biologically plausible convolutional networks. *Advances in Neural Information Processing Systems*, 34:13924–13936, 2021.

A Appendix

A.1 Sparsity in deeper layers

In subsection 4.2 we claimed that in **FF** and **BP/FF** the images of a given category activate consistently a small set of units that we named *ensembles*, that share similarities to what is observed in sensory cortices.

We reported in Figure 1 (Panel **C**) the activation map for Layer 1 (the first hidden layer) of **FF** trained on MNIST data set, and observed that very sparse ensembles emerge. In this Section we show, in a similar fashion, the representations for Layers 2 and 3 (see Figure 5 and Figure 6, respectively). We found that sparsity is preserved across all layers of the network; a similar scenario emerges for the same model trained on FASHIONMNIST and for **BP/FF** on both data sets.

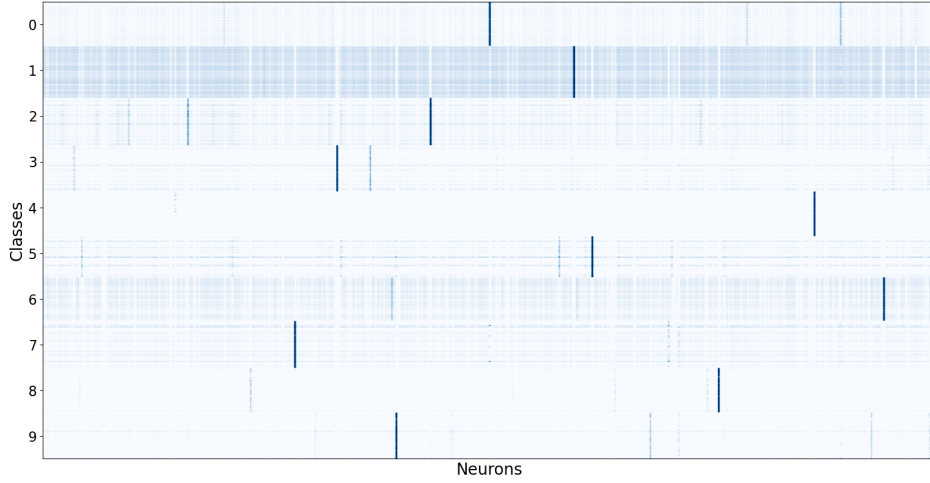


Figure 5: Activation map for Layer 2, across all MNIST test images, grouped by class. A blue dot indicates that an input image activates a certain neuron. Colorscale represents intensity of activation.

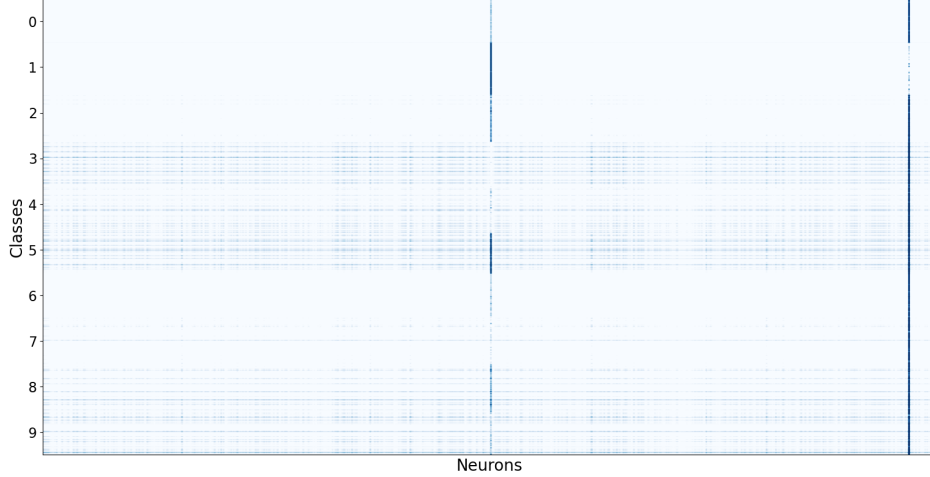


Figure 6: As in Figure 5, activation map for Layer 3 across all MNIST test images, grouped by class.

A.2 Excitatory/inhibitory balance in FF, BP/FF and BP

Let us consider, for a given neuron, the fraction of its positive weights, i.e. the fraction of "excitatory" connections of the afferent neurons. We observed in Section subsection 4.5 that in **FF** the average fraction of positive weights of each neuron in Layer 2 and 3 is remarkably lower with respect to both **BP/FF** and **BP** (see Table 3). On the other hand, we observed in subsection 4.2 (see Figure 2) that the sparsity of **FF** and **BP/FF**, in Layers 1 and 2, is qualitatively comparable and very different from the sparsity observed in **BP**.

When examining the differences between network weights, our attention is primarily directed towards Layers 2 and 3. As mentioned earlier in subsection 4.5, these weights provide us with insights about the emergence of an excitatory/inhibitory mechanism in the neurons. The first hidden layer, through its receptive fields, encodes how the model extracts features from the input and all models show approximately the same fraction of positive and negative values.

In Figure 7 we show that the the average fraction of positive/negative weights follows different distributions in all models we studied. We conclude that the two training protocols of **FF** and **BP/FF** produce models with a profoundly different interplay between excitation and inhibition, despite showing quantitatively similar sparsity levels.

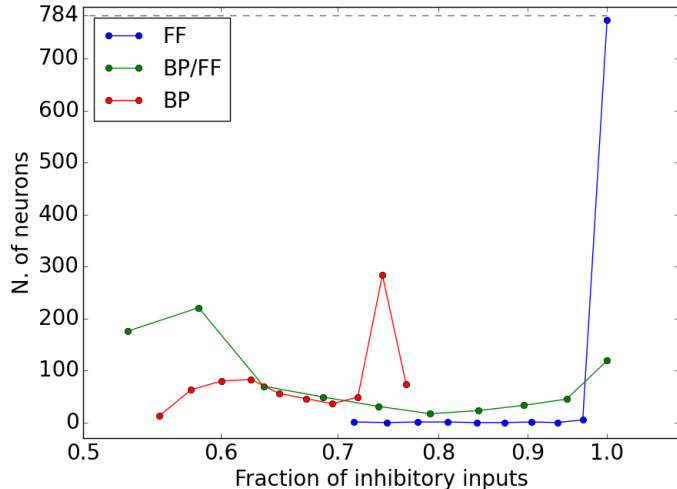


Figure 7: The distribution of the fraction of negative weights (inhibitory connections) of each neuron in Layer 2 of the models **FF**, **BP/FF** and **BP**. In **FF** (blue line), almost all the neurons ($\approx 99\%$, 775 on 784) have 100% negative weights. In **BP/FF** (red line), there is a sharp peak, meaning that nearly $\approx 3/8$ of the neurons have a fraction of inhibitory inputs very close to 75%. Finally, the **BP** model (green curve) shows a relatively even balance between excitatory and inhibitory connections, with a subset of (≈ 100) units in which all inputs are inhibitory. By comparing the histograms of **FF** and **BP/FF** we conclude that the large-scale organization of inhibitory and excitatory connections created by the two training protocols is qualitatively different, despite similar levels of representation sparsity.

A.3 Comparison between methods to define ensembles

In subsection 3.4 we introduced **Methods 1** and **2** to define ensembles, justifying the introduction of the slightly more sophisticated **Method 2** due to its higher sensitivity, useful in the case of the weaker activations produced by unseen categories (see subsection 4.4).

In Figure 8 we show that, despite the results given by the two methods can be, in general, different (Panel **A**) their trends are qualitatively similar (Panel **B**). Therefore, switching from one to the other does not affect any of our main conclusions.

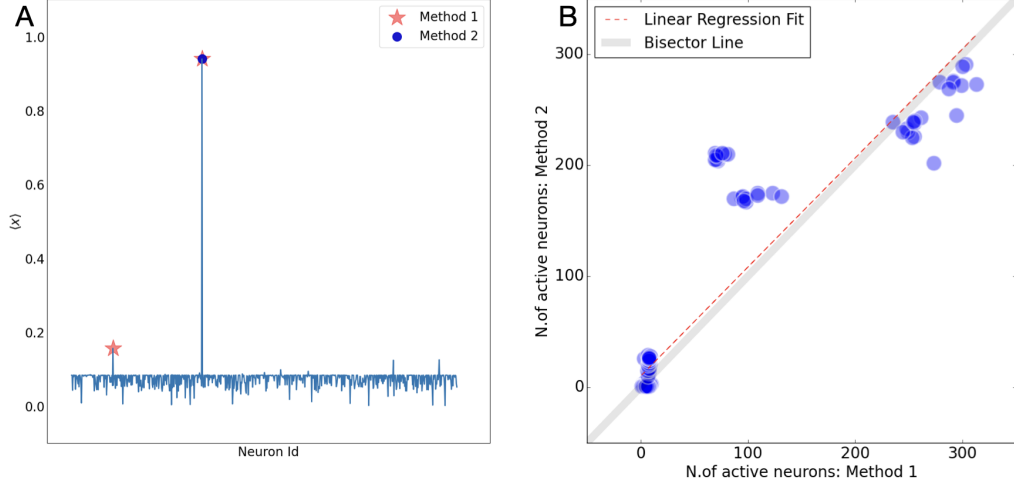


Figure 8: Comparison between **Methods 1** and **2** to define the ensembles. In Panel **A** we show an example in which the two methods give different results. We extracted the activation matrix X of one category and computed the average activation ($\langle x \rangle$) of each neuron (light blue curve). In this case **Method 1** finds two units (red stars) whose activity is prominent, while **Method 2** detects only the unit with the largest average activity. Despite the differences, the two methods give consistent results: in Panel **B** we report the sizes of the ensembles defined by **Method 1** vs. the sizes of the ensembles defined by **Method 2**, for all combinations of models, data sets, categories and layers of our experiments. The linear regression curve (red dashed line) has a slope close to 1 (slope = 0.98, with a non-zero intercept at 9.95). The bisector line is drawn in thick gray, thus showing a strong statistical consistency between the two methods (values used: percentile = 0.99, $\varepsilon = 0.2$).